ACS Photonics

Article

pubs.acs.org/journal/apchd5

InP/InAsP Nanowire-Based Spatially Separate Absorption and Multiplication Avalanche Photodetectors

Vishal Jain,[†,‡] Magnus Heurlin,[†] Enrique Barrigon,[†] Lorenzo Bosco,[†] Ali Nowzari,[†] Shishir Shroff,[†] Virginia Boix,[†] Mohammad Karimi,[†,‡] Reza J. Jam,[†] Alexander Berg,[†] Lars Samuelson,[†] Magnus T. Borgström,[†] Federico Capasso,[§] and Håkan Pettersson*[,†,‡]

[†]Solid State Physics and NanoLund, Lund University, Box 118, SE-221 00 Lund, Sweden

[‡]Laboratory of Mathematics, Physics and Electrical Engineering, Halmstad University, Box 823, SE-301 18 Halmstad, Sweden

[§]School of Engineering and Applied Sciences, Harvard University, Cambridge, Massachusetts 02138, United States

Supporting Information

ABSTRACT: Avalanche photodetectors (APDs) are key components in optical communication systems due to their increased photocurrent gain and short response time as compared to conventional photodetectors. A detector design where the multiplication region is implemented in a large band gap material is desired to avoid detrimental Zener tunneling leakage currents, a concern otherwise in smaller band gap materials required for absorption at 1.3/1.55 μm. Self-assembled III−V semiconductor nanowires offer key advantages such as enhanced absorption due to optical resonance effects, strain-relaxed heterostructures, and compatibility with mainstream silicon technology. Here, we present electrical and optical characteristics of single InP and InP/InAsP nanowire APD structures. Temperature-dependent breakdown characteristics of p^+-n-n^+ InP nanowire devices were investigated first. A clear trap-induced shift in breakdown voltage was inferred from $I-V$ measurements. An improved contact formation to the p^+-InP segment was observed upon annealing, and its effect on breakdown characteristics was investigated. The band gap in the absorption region was subsequently varied from pure InP to InAsP to realize spatially separate absorption and multiplication APDs in heterostructure nanowires. In contrast to the homojunction APDs, no trap-induced shifts were observed for the heterostructure APDs. A gain of 12 was demonstrated for selective optical excitation of the InAsP segment. Additional electron-beam-induced current measurements were carried out to investigate the effect of local excitation along the nanowire on the $I-V$ characteristics. Simulated band profiles and electric field distributions support our interpretation of the experiments. Our results provide important insight for optimization of avalanche photodetector devices based on III−V nanowires.

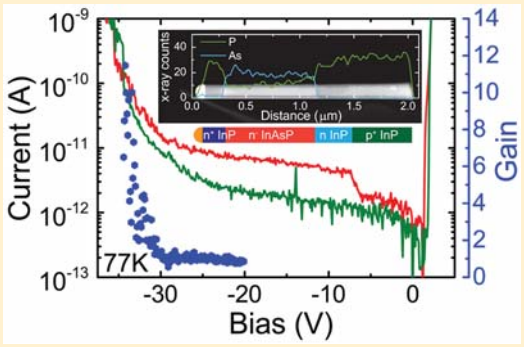

KEYWORDS: *nanowires, avalanche photodetectors, SAM APDs, punch-through*

The research timeline of III−V semiconductor-based avalanche photodetectors (APDs) spans over half a century.[1,2] More recently, improved gain and sensitivity have been attained by shrinking the impact-ionization region in APDs based on nanostructures[3] and nanowires (NWs).[4,5] Furthermore, APDs with absorption in the commercially desired 1.0−1.6 μm wavelength region have also been reported by incorporating quantum heterostructures within the high-electric-field region.[6,7] Properly designed NW arrays have an added advantage of strong nanophotonic resonances, enabling efficient light absorption.[8−10] This has been previously exploited using a plasmonic optical antenna to physically separate the absorption and multiplication regions at the tip and base of the NWs, respectively.[11] When a low band gap material is used for the multiplication region, the devices typically suffer from significant Zener tunneling leakage currents. Therefore, a separate absorption and multiplication (SAM) APD heterojunction structure was proposed four decades ago[12,13] and is nowadays the detector routinely used in long-distance optical communication. This motivated us to develop and now report on the design and realization of the first heterostructure SAM APD implemented in a single NW to date. In these APDs the absorption and multiplication regions are implemented in InAsP, spectrally tuned at 1.55 μm, and InP, respectively. To eliminate possible effects of complex processing in NW arrays, this study entirely focuses on laterally contacted single NW APDs. Our results pave the way for future realization of NW-based array SAM APDs compatible with mainstream silicon technology.

First, a simpler homojunction structure of p^+-n-n^+ InP NWs (sample A) was grown to investigate the breakdown characteristics. This was followed by incorporation of an n^--InAsP absorption segment forming a (p^+-n)-InP-n^--InAsP-n^+-InP

Received: April 17, 2017
Published: October 19, 2017

DOI: 10.1021/acsphotonics.7b00389
ACS Photonics 2017, 4, 2693−2698

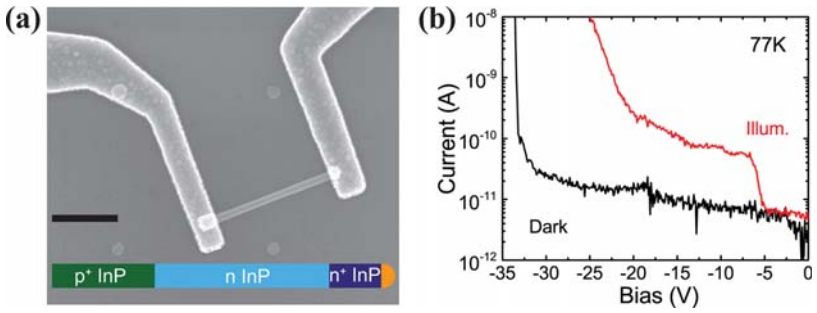

Figure 1. (a) SEM image of a laterally contacted p^+-n-n^+ InP NW device along with the schematics. The scale bar is 1 μm. (b) Avalanche breakdown characteristics of a corresponding device at 77 K under darkness and illumination, respectively.

NW SAM APD (sample B) structure. To obtain statistics from a uniform set of NWs, nanoimprint lithography (NIL) was employed where periodic patterns of circular holes with a diameter of 180 nm and a pitch of 400 nm were prepared on p^+-InP (111)B substrates followed by metal evaporation and lift-off of a 20 nm Au film.[14] An alternative approach to define the gold seed particles in nanosized holes would be to use our recently developed Au electrodeposition technique.[15] Nanowires for different samples were then grown using metal−organic vapor phase epitaxy (MOVPE). Single NWs were mechanically broken off from the as-grown substrates, transferred onto insulating substrates, and laterally contacted (Figure 1a) for optoelectrical characterization (see Methods section for details on sample preparation).

A low dark current (∼10 pA) was recorded for sample A at 77 K before the onset of a breakdown with a 170 mV/decade current rise at a reverse bias of about 33 V (Figure 1b). Several individually contacted single NW devices were studied where the breakdown voltage was found to vary in a range of 31 ± 6 V at 77 K. This range could be an effect of doping variations between different NWs. The breakdown voltage has a positive temperature dependence (Figure S1, Supporting Information) with an estimated temperature coefficient of 50 ± 20 mV/K (measured up to 150 K, clear breakdown characteristics were not observed at higher temperatures) for different devices, which is in agreement with the reported values for bulk InP.[16] Under illumination, at about 7 V reverse bias, we observe a punch-through-like feature where the photocurrent increases by a factor of 10 (Figure 1b). Typically, punch-through is observed when the depletion region extends to the edge of the absorption layer in heterostructure SAM APDs. In the present case of homojunction InP APDs, only a small photocurrent (PC) contribution is observed below 5 V reverse bias. We attribute this to a significant recombination of photogenerated electron−hole pairs via Shockley−Read−Hall states in the band gap. The observed punch-through marks the onset of enhanced carrier collection of photogenerated electron−hole pairs as the electric field increases in a fully depleted n-segment, as well as of holes diffusing from the n^+-segment under illumination. It should be mentioned that the diffusion length of holes is <50 nm estimated from standard tabulated electron and hole mobilities in bulk InP and the experimentally determined electron diffusion length of about 150−200 nm.[17,18] Figure S2 (Supporting Information) shows the theoretically calculated band profiles and electric field distributions for various biases at 300 K. Assuming nominal doping profiles, Figure S2b (Supporting Information) indeed shows that the depletion region approximately reaches the n^+-segment, and the electric field vanishes at the same point, at −7 V, in agreement with the experimentally observed step in the experimental data in Figure 1b. An approximate unity gain responsivity of about 5 A/W can be estimated after punch-through from the ∼100 pA current level under illumination with an intensity of 5 mW/cm^2. We note that the breakdown voltage of about −25 V under illumination is significantly lower than under dark conditions. A similar voltage shift is in fact typically observed in darkness when the $I-V$ characteristic is reswept after the initial sweep (Figure S1, Supporting Information). Subsequent sweeps, however, do not result in any further significant shifts, and the $I-V$ characteristics remain constant. We attribute the observed voltage shift to filling of hole-traps after the first sweep, thereby increasing the effective space charge density and thus reducing the bias required to obtain the high electric field necessary for breakdown. A similar effect has been reported in the case of SiC avalanche diodes.[19] The effect of traps is also clearly visible under power-dependent laser excitation (532 nm) where the photocurrent saturates at higher laser power (Figure S3, Supporting Information). The observed voltage shift unfortunately makes it impossible to identify a well-defined unity gain baseline required to properly calculate the gain. Further studies, beyond the scope of this work, are needed to unravel the physical origin of these hole-traps and their influence on the trapping and recombination mechanisms discussed above. Figure S2c (Supporting Information) shows the electric field distribution at the approximate breakdown voltage of −25 V after resweep of the bias (Figure S1, Supporting Information). It should be noted that the maximum electric field of about (3−4) × 10^7 V/m in Figure S2c is in reasonable agreement with tabulated breakdown fields for InP at the doping levels of our devices.[20]

An interesting observation is the effect of wafer dimensions on the breakdown characteristics. For each growth run, we placed two Au catalyst imprinted samples of different sizes in the MOVPE chamber. It was found that the NWs obtained from the smaller sample showed a much higher breakdown voltage (67 ± 16 V at 77 K) compared to the NWs discussed above (31 ± 6 V at 77 K). We attribute this observation to a larger edge effect for the smaller sample, which results in longer NWs (2.2−2.4 μm in this case compared to 1.6−1.8 μm in the previous set), which in turn is a result of more In being present close to the sample edges. A higher amount of In reduces the Sn dopant incorporation[21] and thereby increases the bias required to obtain sufficiently high electric fields for impact ionization.

After the investigation of the homojunction InP APDs, heterostructure APDs (sample B) were realized by changing the

DOI: 10.1021/acsphotonics.7b00389
ACS Photonics 2017, 4, 2693−2698

material in the absorption region from InP to InAsP by tuning the As composition (see Methods section for details). From TEM investigations it was concluded that the grown InAsP segment is predominantly wurtzite with an almost constant As concentration of 63 ± 2%. We also found a 100 nm long segment next to the n-InP segment where the As concentration was 53 ± 2% (Figure 2a). Although this segment was not

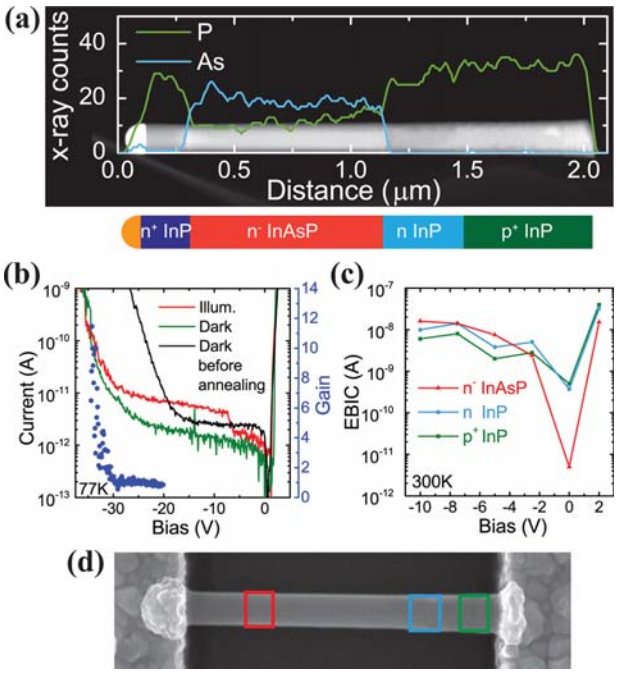

Figure 2. (a) EDX linescans superimposed on a TEM image, along with a schematic of an InP/InAsP NW SAM APD (sample B). (b) *I*−*V* characteristics and gain at 77 K of an InP/InAsP NW SAM APD in the dark, before and after annealing, and under selective illumination of the InAsP absorption region. (c) Electron-beam-induced current (EBIC) versus bias characteristics corresponding to e-beam excitation in (d). (d) Spatially resolved e-beam excitation map over the length of the NW.

intended, it can increase the efficiency of hole extraction from the absorption segment since the valence band discontinuity between the absorption and multiplication segment is reduced.[22] The grown NWs were transferred to Au-patterned Si substrates for photoluminescence (PL) measurements at 4 K. PL signals corresponding to the InP regions and n^--$InAs_{0.63}P_{0.37}$ absorption region were observed at about 0.90 and 1.55 μm at 4 K (Figure S4, Supporting Information). In addition we measured a significant PL signal in the 1.2−1.4 μm range, the origin of which is unclear at this point. A comparative PL spectrum from an InP APD shows no such peaks, which rules out the possibility of dopant-related defects. The rather sharp peaks most likely originate from defects at the InP−InAsP interface. Further studies using characterization techniques like cathodoluminescence spectroscopy are needed to unravel the origin of these peaks. We point out, however, that these defects do not seem to affect the device performance, as evident from the discussions below.

The contacted SAM APDs in general showed less sharp breakdown characteristics (Figure 2b) compared to InP APDs, even at 77 K. This might be attributed to an increased Zener tunneling leakage current due to the smaller band gap (E_g = 0.8 eV) of InAsP after the electric field punches through into this region, in spite of our efforts to tailor the electric field distribution (doping profile) to suppress such breakdown mechanisms.[13] Interestingly, these devices exhibited minimal shift in *I*−*V* characteristics in subsequent sweeps (Figure S5, Supporting Information), indicating that the previously observed trapping effects are associated with InP. They do, however, show similar breakdown voltage shifts upon annealing (Figure 2b) as in the case of the InP APDs. For illumination, a quartz lamp with a silicon long-pass filter was used to selectively illuminate the InAsP absorption region.

The depletion region reaches the InAsP absorption segment at a punch-through bias of −8 V, in agreement with the theoretically calculated band profiles and electric field distributions for various biases and nominal doping levels shown in Figure 3. Figure 3a shows the schematic energy band

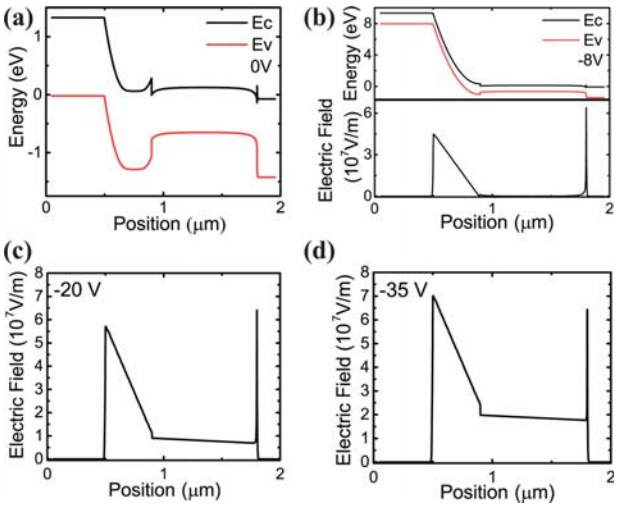

Figure 3. Characteristics of the InAsP SAM APD at 300 K: (a) Band profile at 0 V. (b) Band profile at punch-through (−8 V, upper panel) and corresponding electric field distribution (lower panel). (c) Electric field distribution at −20 V. (d) Electric field distributions at the approximate breakdown voltage of −35 V.

diagram at thermal equilibrium. Figure 3b shows the band diagram and electric field distribution at −8 V, confirming the penetration of the depletion region to the edge of the InAsP absorption segment. This bias is in agreement with the bias at which the large step in PC is observed in Figure 2b due to the increased collection of photogenerated holes in the InAsP segment of the NW. To calculate the gain shown as blue dots in Figure 2b, we first plot the *I*−*V* under illumination (red trace) after subtracting the dark current (green trace) in a linear scale (not shown). This resulting PC first increases smoothly (sublinearly) with reverse bias V reflecting the enhanced collection of photogenerated holes by the expanding depletion region. We define this smoothly increasing PC signal as the unity gain line $PC_{UG}(V)$. Above about −28 V, the $PC(V)$ takes off from the extracted unity gain line. The gain, $G(V)$, is subsequently calculated at each bias according to $G(V) = PC(V)/PC_{UG}(V)$.[23] From this analysis we derive a maximum gain of about 12. Moreover, from the estimated infrared intensity of about 15 mW/cm^2 in this spectral region, we calculate a maximum unity gain responsivity of 0.15 A/W. It is worth mentioning here that a quartz lamp was used in these experiments instead of a high-power laser to demonstrate the

DOI: 10.1021/acsphotonics.7b00389
ACS Photonics 2017, 4, 2693−2698

usability of the NW-based APDs. Almost no increase in total current was observed upon illumination with a quartz lamp without the silicon long-pass filter for reverse biases below the punch-through region (Figure S6, Supporting Information), which indicates that the carriers are selectively generated and collected from the InAsP absorption region. Figure 3c shows the calculated electric field at −20 V showing an enhanced electric field throughout the fully depleted InAsP region. Figure 3d shows the electric field distribution at the estimated breakdown voltage of about −35 V (Figure 2b). The electric field at the InAsP/n-InP interface amounts to about 2×10^7 V/m. At this field, Zener tunneling in the low band gap InAsP segment will contribute significantly to the $I-V$ near breakdown, combined with impact ionization in the InP avalanche region.[24]

A further conclusive verification of selective generation and collection of carriers in the InAsP absorption region was done through selective spatial excitation with an e^--beam (Figure 2c and d). Exciting the p^+-InP or n-InP region yielded similar low current levels at zero or forward biases, but with a slightly enhanced drift-induced carrier collection at reverse biases when bombarding the n-InP region with electrons. Exciting the n^--InAsP region generated significantly lower current levels at zero bias due to the InP/InAsP heterojunction barrier faced by the holes, which is more easily overcome at forward bias. Interestingly, the EBIC signal increased by a factor of 4 at 10 V with respect to 2 V reverse bias, similar to the photocurrent increase under punch-through conditions.

In conclusion, we have studied avalanche breakdown characteristics of single NW InP APDs. Annealing the samples at 350 °C significantly improved the contact to p^+-InP and increased the breakdown voltage. A clear effect of trap states on the breakdown characteristics was evident, and a detailed study is needed to investigate the trap mechanism. The main result of the work is the first demonstration of InP/InAsP NW SAM APDs with spectrally tuned absorption at 1.55 μm. Studies of selective excitation of the absorption region using both photons and electrons yielded consistent results and a multiplication gain of up to 12. These devices are ideal candidates for future development of NW-based array SAM APDs.

METHODS

Growth. NW growth for sample A was carried out in a low-pressure (100 mbar) MOVPE system (Aixtron 200/4), with a total flow of 13 L/min using hydrogen (H_2) as carrier gas. Trimethylindium (TMI), arsine (AsH_3), and phosphine (PH_3) were used as precursors for NW growth, while diethylzinc (DEZn) and tetraethyltin (TESn) were used as p-dopant[17] and n-dopant[25] precursors, respectively. Hydrogen chloride (HCl) at a molar fraction of $\chi_{HCl} = 6.1 \times 10^{-5}$ was used to inhibit the radial growth.[26] Before growth, the samples were first annealed at 550 °C for 10 min under a PH_3/H_2 gas mixture to desorb any surface oxides at a constant molar fraction of $\chi_{PH3} = 6.9 \times 10^{-3}$. In this step the Au discs defined by NIL turn into 130 nm diameter catalyst nanoparticles. The reactor was then cooled to 440 °C, at which point growth was initiated by the addition of TMI and DEZn to the gas flow at molar fractions of $\chi_{TMI} = 7.4 \times 10^{-5}$ and $\chi_{DEZn} = 6.1 \times 10^{-5}$ and lowering χ_{PH3} to 1.5×10^{-3}. After a 30 s nucleation time, HCl was introduced and χ_{PH3} was increased to 6.9×10^{-3}. The grown InP p^+-segment has a nominal acceptor concentration of about 5×10^{18} cm^{-3}.[17] For the n-segment, TESn was used at a molar fraction of $\chi_{TESn} = 3.5 \times 10^{-7}$, resulting in an estimated doping concentration of (1−5) $\times 10^{16}$ cm^{-3} based on previous studies.[25,27,28] For the top n^+-segment growth, $\chi_{TESn} = 4.8 \times 10^{-6}$ along with a reduced TMI flow rate ($\chi_{TMI} = 5.2 \times 10^{-5}$) was used to effectively increase the Sn incorporation[21] to an estimated doping level higher than 5×10^{18} cm^{-3}.[28] After completing the top n^+-segment, the growth was terminated and the sample cooled in a PH_3/H_2 gas mixture. The grown p^+-n-n^+ InP NWs had a diameter of 130 nm and average segment lengths of approximately 500/1100/350 nm for a growth time of 2/6/9 min, respectively, measured using an in situ optical reflectance characterization setup.[29]

The same growth parameters as for sample A were used to grow a 500 nm (2 min) p^+-InP segment and a 400 nm (2 min) n-InP avalanche segment for the InAsP/InP NW SAM APD. To maintain an almost constant As concentration in the 900 nm (8 min) n^--InAsP segment, the AsH_3 flow was ramped from a molar fraction of $\chi_{AsH3} = 2.3 \times 10^{-4}$ to $\chi_{AsH3} = 1.2 \times 10^{-4}$. To compensate for the lower etch rate of InAsP as compared to InP, the HCl flow was increased to a molar fraction of $\chi_{HCl} = 6.1 \times 10^{-5}$, thereby reducing tapering of the NWs. A reduced flow of TESn at a molar fraction of $\chi_{TESn} = 3.5 \times 10^{-8}$ resulted in an estimated doping concentration of (5−8) $\times 10^{15}$ cm^{-3}.[25,27] The gas flows were finally switched back to the same parameters used for the growth of the top n^+-InP segment in sample A, but resulting in a shorter 140 nm long n^+-InP segment.

Device Fabrication. For electrical measurements, single NWs were mechanically transferred to n-type Si substrates coated with 100 nm thermal SiO_2 and 12 nm HfO_2. The samples were spin-coated with PMMA 950A5 at 5000 rpm followed by a 5 min hot-plate bake at 180 °C. The contact regions to the NW ends were exposed using a Raith 150 EBL system, with subsequent pattern development in an MIBK:IPA 1:3 solution for 1 min. Then a multilayer of Pd/Zn/Pd/Au was thermally evaporated with thicknesses of 2/20/68/110 nm, respectively, and removed from unexposed areas through lift-off in acetone. Figure 1a shows an SEM image of a fabricated device.

It is well known that ohmic contacts are difficult to obtain to p^+-InP.[30] It has been demonstrated that an annealing step above 420 °C allows Zn from the metal contact to diffuse into the InP NWs, which significantly improves the contact properties.[31] This approach has previously also been used for p^+-InP NWs.[32] Annealing above 350 °C, however, led to changes in surface morphology in our NW devices (Figure S7, Supporting Information). The contact to the p^+-InP segment in our devices was thus activated by a rapid thermal annealing process at 350 °C for 30 s. This temperature is typically not high enough for Zn to diffuse into the NWs,[31,33] which is one reason that Pd/Zn/Pd/Au layers have also been used for ohmic contacts to n-InP.[32] We however measured a substantial decrease in contact resistance between two nearby Pd/Zn/Pd/Au contacts to the p^+-InP segment from 3.8×10^{-3} Ωcm^2 to 6.6×10^{-4} Ωcm^2 after annealing (Figure S8a, Supporting Information). This contact resistance effect was further studied using e^--beam-induced current (EBIC) measurements. Before annealing, the EBIC signal from the Schottky contact between the Pd/Zn/Pd/Au contact and p^+-InP segment was dominant, whereas the effective p^+-n junction in the NW was clearly visible after annealing (Figure S8c and d, Supporting Information). The p^+-n junction boundary observed at a distance of 200 nm from the metal contact (Figure S8c, Supporting Information) is reasonable considering that out of

DOI: 10.1021/acsphotonics.7b00389
ACS Photonics 2017, 4, 2693−2698

the 500 nm p^+-InP segment about 190 nm is buried under the metal contact and about 60−90 nm of the NW base is left as a stub on the as-grown substrate after transferring the NWs (Figure S9, Supporting Information). The annealing step further led to an increase in the observed breakdown voltage (Figure 3b). We can only speculate that Zn dopant diffusion might act as a compensatory dopant in the adjacent n-InP segment, thus requiring a higher applied bias to achieve the necessary electric field.

Measurements. The $I-V$ characteristics of the contacted NWs were measured with a Keithley 6430 sub-femtoampere sourcemeter with the samples mounted inside a Janis PTSHI-950-FTIR pulse-tube closed-cycle cryostat integrated with a Bruker Vertex 80 V Fourier transform infrared (FTIR) spectrometer. The built-in quartz lamp in the FTIR was used as the light source for recording the $I-V$ under illumination.

Modeling. The band-structure and electric field modeling were performed using Lumerical software. The steady-state solver mode was employed in auto refinement mode with a maximum number of refinement steps of 2×10^4 and with a minimum edge length of 0.001 μm as global mesh constraints. The geometry included nominal segment lengths, compositions, and doping concentration profiles as described previously in the paper.

■ ASSOCIATED CONTENT

Supporting Information

The Supporting Information is available free of charge on the ACS Publications website at DOI: 10.1021/acsphotonics.7b00389.

Temperature-dependent $I-V$ characteristics of InP NW APDs, simulated electrostatics of InP APDs and $I-V$ characteristics of InP NW APDs under different laser power; PL spectra of InP/InAsP NW SAM APDs, corresponding $I-V$ characteristics after successive voltage sweeps, and $I-V$ characteristics under illumination with and without Si filter; SEM images of InP NW APDs with corresponding $I-V$ characteristics and EBIC after annealing; SEM image of the substrate after mechanical transferring of NWs (PDF)

■ AUTHOR INFORMATION

Corresponding Author

*E-mail: hakan.pettersson@hh.se.

ORCID

Mohammad Karimi: 0000-0002-3160-8540

Magnus T. Borgström: 0000-0001-8061-0746

Håkan Pettersson: 0000-0001-5027-1456

Author Contributions

All authors have given approval to the final version of the manuscript.

Notes

The authors declare no competing financial interest.

■ ACKNOWLEDGMENTS

The authors acknowledge financial support from NanoLund, the Swedish Research Council, the Swedish National Board for Industrial and Technological Development, the Swedish Foundation for Strategic Research, the Ljungberg Foundation, the Carl Trygger Foundation, and the Swedish Energy Agency. This project has received funding from the European Union's Horizon 2020 research and innovation program under grant agreement No. 641023 (NanoTandem) and under the Marie Sklodowska-Curie grant agreement No. 656208.

■ REFERENCES

(1) McIntyre, R. J. Multiplication Noise in Uniform Avalanche Diodes. *IEEE Trans. Electron Devices* **1966**, *13*, 164−168.

(2) Campbell, J. C. Recent Advances in Telecommunications Avalanche Photodiodes. *J. Lightwave Technol.* **2007**, *25*, 109−121.

(3) Assefa, S.; Xia, F.; Vlasov, Y. A. Reinventing germanium avalanche photodetector for nanophotonic on-chip optical interconnects. *Nature* **2010**, *464*, 80−84.

(4) Hayden, O.; Agarwal, R.; Lieber, C. M. Nanoscale avalanche photodiodes for highly sensitive and spatially resolved photon detection. *Nat. Mater.* **2006**, *5*, 352−356.

(5) Yang, C.; Barrelet, C. J.; Capasso, F.; Lieber, C. M. Single p-Type/Intrinsic/n-Type Silicon Nanowires as Nanoscale Avalanche Photodetectors. *Nano Lett.* **2006**, *6*, 2929−2934.

(6) Bulgarini, G.; Reimer, M. E.; Hocevar, M.; Bakkers, E. P. A. M.; Kouwenhoven, L. P.; Zwiller, V. Avalanche amplification of a single exciton in a semiconductor nanowire. *Nat. Photonics* **2012**, *6*, 455−458.

(7) Chuang, L. C.; Sedgwick, F. G.; Chen, R.; Ko, W. S.; Moewe, M.; Ng, K. W.; Tran, T.-T. D.; Chang-Hasnain, C. GaAs-Based Nanoneedle Light Emitting Diode and Avalanche Photodiode Monolithically Integrated on a Silicon Substrate. *Nano Lett.* **2011**, *11*, 385−390.

(8) Wallentin, J.; Anttu, N.; Asoli, D.; Huffman, M.; Åberg, I.; Magnusson, M. H.; Siefer, G.; Fuss-Kailuweit, P.; Dimroth, F.; Witzigmann, B.; Xu, H. Q.; Samuelson, L.; Deppert, K.; Borgström, M. T. InP Nanowire Array Solar Cells Achieving 13.8% Efficiency by Exceeding the Ray Optics Limit. *Science* **2013**, *339*, 1057−1060.

(9) Svensson, J.; Anttu, N.; Vainorius, N.; Borg, B. M.; Wernersson, L. E. Diameter-dependent photocurrent in InAsSb nanowire infrared photodetectors. *Nano Lett.* **2013**, *13*, 1380−1385.

(10) Nowzari, A.; Heurlin, M.; Jain, V.; Storm, K.; Hosseinnia, A.; Anttu, N.; Borgström, M. T.; Pettersson, H.; Samuelson, L. A comparative study of absorption in vertically and laterally oriented InP core-shell nanowire photovoltaic devices. *Nano Lett.* **2015**, *15*, 1809−1814.

(11) Farrell, A. C.; Senanayake, P.; Hung, C.-H.; El-Howayek, G.; Rajagopal, A.; Currie, M.; Hayat, M. M.; Huffaker, D. L. Plasmonic field confinement for separate absorption-multiplication in InGaAs nanopillar avalanche photodiodes. *Sci. Rep.* **2015**, *5*, 17580.

(12) Nishida, K.; Taguchi, K.; Matsumoto, Y. InGaAsP heterostructure avalanche photodiodes with high avalanche gain. *Appl. Phys. Lett.* **1979**, *35*, 251−252.

(13) Kim, O. K.; Forrest, S. R.; Bonner, W. A.; Smith, R. G., A high gain In0.53Ga0.47As/InP avalanche photodiode with no tunneling leakage current. *Appl. Phys. Lett.* **1981**, *39*, 40210.1063/1.92752.

(14) Otnes, G.; Heurlin, M.; Graczyk, M.; Wallentin, J.; Jacobsson, D.; Berg, A.; Maximov, I.; Borgström, M. T. Strategies to obtain pattern fidelity in nanowire growth from large-area surfaces patterned using nanoimprint lithography. *Nano Res.* **2016**, *9*, 2852−2861.

(15) Jam, R. J.; Heurlin, M.; Jain, V.; Kvennefors, A.; Graczyk, M.; Maximov, I.; Borgström, M. T.; Pettersson, H.; Samuelson, L. III−V Nanowire Synthesis by Use of Electrodeposited Gold Particles. *Nano Lett.* **2015**, *15*, 134−138.

(16) Tan, L. J. J.; Ong, D. S. G.; Ng, J. S.; Tan, C. H.; Jones, S. K.; Qian, Y.; David, J. P. R. Temperature Dependence of Avalanche Breakdown in InP and InAlAs. *IEEE J. Quantum Electron.* **2010**, *46*, 1153−1157.

(17) Wallentin, J.; Wickert, P.; Ek, M.; Gustafsson, A.; Wallenberg, L. R.; Magnusson, M. H.; Samuelson, L.; Deppert, K.; Borgström, M. T. Degenerate p-doping of InP nanowires for large area tunnel diodes. *Appl. Phys. Lett.* **2011**, *99*, 253105.

(18) Jain, V.; Nowzari, A.; Wallentin, J.; Borgström, M. T.; Messing, M. E.; Asoli, D.; Graczyk, M.; Witzigmann, B.; Capasso, F.; Samuelson,

DOI: 10.1021/acsphotonics.7b00389
ACS Photonics 2017, 4, 2693−2698

L. Study of photocurrent generation in InP nanowire-based p^+-i-n^+ photodetectors. *Nano Res.* **2014**, *7*, 544−552.
(19) Liu, S.; Yang, C.; Sun, W.; Qian, Q.; Huang, Y.; Wu, X.; Wu, M.; Yang, Q.; Sun, L. Repetitive-Avalanche-Induced Electrical Parameters Shift for 4H-SiC Junction Barrier Schottky Diode. *IEEE Trans. Electron Devices* **2015**, *62*, 601−605.
(20) Kyuregyan, A. S.; Yurkov, S. N. Room-temperature avalanche breakdown voltages of Si, Ge, SiC, GaAs, GaP and InP. *Sov. Phys. Semicond.* **1989**, *23*, 1126−1132.
(21) Lindelöw, F.; Heurlin, M.; Otnes, G.; Dagyte, V.; Hultin, O.; Storm, K.; Samuelson, L.; Borgström, M. Doping evaluation of InP nanowires for tandem junction solar cells. *Nanotechnology* **2016**, *27*, 065706.
(22) Campbell, J. C.; Holden, W. S.; Qua, G. J.; Dentai, A. G. Frequency Response of InP/InGaAsP/InGaAs Avalanche Photodiodes with Separate Absorption "Grading" and Multiplication Regions. *IEEE J. Quantum Electron.* **1985**, *21*, 1743−1746.
(23) Yuan, P.; Anselm, K. A.; Hu, C.; Nie, H.; Lenox, C.; Holmes, A. L.; Streetman, B. G.; Campbell, J. C.; McIntyre, R. J. A new look at impact ionization-Part II: Gain and noise in short avalanche photodiodes. *IEEE Trans. Electron Devices* **1999**, *46*, 1632−1639.
(24) Forrest, S. R.; Smith, R.; Kim, O. Performance of $In_{0.53}Ga_{0.47}As$/InP avalanche photodiodes. *IEEE J. Quantum Electron.* **1982**, *18*, 2040−2048.
(25) Borgström, M. T.; Norberg, E.; Wickert, P.; Nilsson, H. A.; Trägårdh, J.; Dick, K. A.; Statkute, G.; Ramvall, P.; Deppert, K.; Samuelson, L. Precurson evaluation for in situ InP nanowire doping. *Nanotechnology* **2008**, *19*, 5602.
(26) Borgström, M. T.; Wallentin, J.; Trägårdh, J.; Ramvall, P.; Ek, M.; Wallenberg, L. R.; Samuelson, L.; Deppert, K. In-situ etching for total control over axial and radial nanowire growth. *Nano Res.* **2010**, *3*, 264−270.
(27) Wallentin, J.; Ek, M.; Wallenberg, L. R.; Samuelson, L.; Borgström, M. T. Electron Trapping in InP Nanowire FETs with Stacking Faults. *Nano Lett.* **2012**, *12*, 151−155.
(28) Jain, V.; Heurlin, M.; Karimi, M.; Hussain, L.; Aghaeipour, M.; Nowzari, A.; Berg, A.; Nylund, G.; Capasso, F.; Samuelson, L.; Borgström, M. T.; Pettersson, H. Bias-dependent spectral tuning in InP nanowire-based photodetectors. *Nanotechnology* **2017**, *28*, 114006.
(29) Heurlin, M.; Anttu, N.; Camus, C.; Samuelson, L.; Borgström, M. T. In Situ Characterization of Nanowire Dimensions and Growth Dynamics by Optical Reflectance. *Nano Lett.* **2015**, *15*, 3597−3602.
(30) Kuphal, E. Low resistance ohmic contacts to n- and p-InP. *Solid-State Electron.* **1980**, *24*, 69−78.
(31) Ivey, D. G.; Jian, P.; Wan, L. Pd/Zn/Pd/Au Ohmic Contacts to p-Type InP. *J. Electron. Mater.* **1991**, *20*, 237−246.
(32) Storm, K.; Nylund, G.; Borgström, M.; Wallentin, J.; Fasth, C.; Thelander, C.; Samuelson, L. Gate-Induced Fermi Level Tuning in InP Nanowires at Efficiency Close to the Thermal Limit. *Nano Lett.* **2011**, *11*, 1127−1130.
(33) Hwang, S.; Shim, J.; Eo, Y. Ohmic contacts of Pd/Zn/M(=Pd or Pt)/Au to p-type InP. *J. Kor. Phys. Soc.* **2005**, *46*.

DOI: 10.1021/acsphotonics.7b00389
ACS Photonics 2017, 4, 2693−2698